Determination of the Complete Set of Iron Normal Modes in the Heme Model Compound Fe^{III}(OEP)Cl from Nuclear Resonance Vibrational Spectroscopic Data

Timo E. Budarz, E. W. Prohofsky, and Stephen M. Durbin*

Department of Physics, Purdue University, West Lafayette, Indiana 47907

Theodore Sjodin and J. Timothy Sage

Department of Physics, Northeastern University, Boston, Massachusetts 02115

Wolfgang Sturhahn and E. Ercan Alp

Advanced Photon Source, Argonne National Laboratory, Argonne, Illinois 60439

Received: October 30, 2002; In Final Form: July 21, 2003

The vibrational spectrum of ^{57}Fe in chloro iron octaethylporphyrin, Fe(OEP)Cl, has been calculated by normal-mode analysis refined to absorption data from nuclear resonance vibrational spectroscopy. This technique directly measures the amplitudes and frequencies for all modes that have significant iron participation, providing rigorous constraints to the best-fit values for the force constants. The calculated normal modes reveal the importance of Fe displacements perpendicular to the heme plane for both the lowest frequency modes and the ligand modes. The actual normal modes of Fe(OEP)Cl are not well described by single modes of the core porphyrin; instead they are hybrids of multiple core modes and ethyl and chlorine displacements.

I. Introduction

Approximately one-third of all proteins include metal ions that serve either functional or structural roles.[1] Proteins such as hemoglobin, myoglobin, neuroglobin, and the various cytochromes all have metalloporphyrins at their active sites.[2−4] In hemoglobin and myoglobin, for example, the heme iron is part of the oxygen transport function. We report here on investigations of the model compound chloro iron octaphenylporphyrin, Fe(OEP)Cl, as a step in understanding biologically significant dynamics in heme proteins. This follows similar work done on nitrosyl iron tetraphenylporphyrin, Fe(TPP)NO,[5] and Fe(TPP)-(2-MeHIm).[6]

We employ normal-mode analysis to calculate the ^{57}Fe partial vibrational density of states (VDOS) and refine the force field until a good fit to the experimental results from nuclear resonance vibrational spectroscopy (NRVS) is achieved.

Previous studies of porphyrin dynamics have mainly focused on resonance Raman (RR) and infrared (IR) techniques. Only a subset of modes can be observed by these techniques because of optical selection rules. It is also difficult to assign experimental peaks to normal modes with specific atomic displacements. Isotopic substitution has been successfully used to determine the character of certain vibrational modes, since the frequency shift of a mode can be attributed to the change in mass of a specific atom. This technique is problematic for modes below a few hundred wavenumbers since they include displacements of many different atoms. This reduces the consequent shift in frequency as it is the total mass of all atoms moving in the mode that is important for frequency shift. Change in mass (isotopic substitution) of one atom only changes this mass by a small amount. In the same way, neither IR nor RR can be used to match spectral peak amplitude to the amplitude of the vibrational motion since the electron−phonon interaction terms are not well enough known.

NRVS is not subject to optical selection rules. It is sensitive to any motion of ^{57}Fe atoms along the direction of the X-ray probe beam. The spectrum contains the frequency as well as the amplitude of the iron motion that can be used in refinement of the force constants, and ultimately in making assignments. The absence of optical selection rules gives, in essence, many more data to use in refinement. The certainty that the spectral data comes exclusively from Fe motion makes the optimization of molecular force constants to fit the experimental data much simpler and more effective.

II. Sample Preparation

Fe(OEP)Cl with enrichment of 91% ^{57}Fe was purchased in polycrystalline powder form from Midcentury Chemical Company, and was used without further refinement. Approximately 30 mg of this material was mixed with a small amount of vacuum grease and placed in a sample cell with a thin Mylar window to permit incident X-rays to reach the sample and subsequent ^{57}Fe X-ray fluorescence to leave with minimal absorption. This cell was placed in an evacuated cryostat, cooled by flowing liquid helium. The average sample temperature during data collection was 87 K, as determined from the NRVS data.

III. NRVS

Nuclear resonance vibrational spectroscopy has been described in detail elsewhere.[7−11] Briefly, the absorption of a highly monochromatic X-ray beam is monitored as the energy is scanned near the nuclear resonance of Mössbauer-active ^{57}Fe. Resonant absorption of X-rays by the nucleus can occur when the X-ray energy E_x is within the exceedingly narrow Mössbauer line width (about 10^{-8} eV) of the resonance E_o. If the difference between E_x and E_o matches the energy of a

10.1021/jp027348w CCC: $25.00
Published on Web 09/16/2003

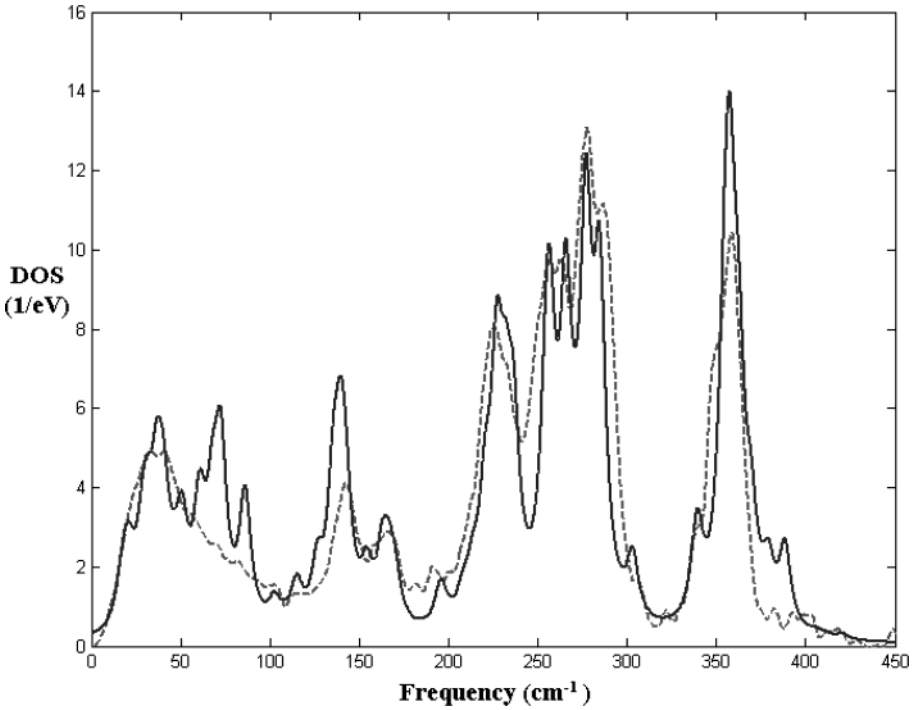

Figure 1. Comparison of experimental (solid line) density of states (DOS) to calculated and refined (dashed line) DOS. The discrepancy in various amplitudes is attributed to intermolecular interactions that are not accounted for in the single-molecule model used in the calculation (see section III). (The calculated DOS is multiplied by an arbitrary scaling factor.).

vibrational quantum (phonon) of the system E_{vib}, absorption can occur off resonance. Off-resonance absorption must be assisted by the creation or annihilation of phonons (Stokes and anti-Stokes processes), endowing the absorption spectrum with detailed information on the vibrational density of states. NRVS is completely specific to the resonant ^{57}Fe nuclei in this sample since it is the only Mössbauer active species present, and therefore only ^{57}Fe vibrational motion contributes to the measured spectrum, greatly simplifying mode assignment. The ^{57}Fe enrichment of 91% in this sample was an essential step for reasonable data collection time, which was 2−4 h.

The measurements were made in sector 3-ID of SRI-CAT at the Advanced Photon Source, Argonne National Laboratory. An energy resolution of 0.85 meV and a photon flux of approximately 1 GHz (necessary to get reasonable count rates) at 14.414 keV (^{57}Fe nuclear resonance) were obtained by using a diamond premonochromator followed by a dispersive pair of asymmetric 975 Si crystals.[12] The beam energy was scanned above and below the nuclear excitation energy of the ^{57}Fe, and the time-delayed ^{57}Fe atomic K fluorescence was monitored as a signal of nuclear absorption. Absorption data were converted to the Fe vibrational density of states (VDOS) using the PHOENIX program developed by Sturhahn.[13]

The experimental spectrum has several distinct features (Figure 1). The force field was optimized to match the calculated spectrum to the experimental spectrum in the range of the NRVS data (Table 1). With the exception of modes below approximately 100 cm^{-1}, the experimental features have a line width dictated by the experimental resolution of 8 cm^{-1}. Below 100 cm^{-1} there is increased dispersion in the data, presumably due to intermolecular effects. Since the calculation was done using a single-molecule model, it does not include this line broadening or contributions from acoustic modes. The calculated normal modes were given 8 cm^{-1} Lorentzian line widths (experimental resolution) to produce a vibrational density of states that can be compared directly with the data.

TABLE 1: Selected Force Constants from the Refined Force Field[a]

stretch	force const (mdyn/Å)	bend	force const (mdyn/rad)
Fe−Cl	1.14	N−Fe−Cl	0.32
Fe−N	0.97	Fe−N−C_α	0.33
N−C_α	5.30	N−C_α−C_β	1.50
C−H_E	4.10	N−C_α−C_m	0.65
C_α−C_β	4.89	C_α−C_β−C_β	1.11
C_α−C_m	6.24	C_α−C_β−C_1	1.08
C_β−C_β	6.61		
C_β−C_1	4.68		
C_1–C_2	4.10		

[a] The listed values are an average from the four quadrants in the molecule.

IV. Normal-Mode Analysis

Calculations were performed on a desktop PC (Athlon 1000 MHz) running software written by our group for the purpose of normal-mode calculations and optimal refinement of the molecular force field. Total processor time was 3−5 h.

Fe(OEP)Cl was modeled as a 58-atom molecule (see Figure 2). The three hydrogen atoms bonded to each of the outer carbon atoms on the ethyl groups were left out, and their masses were added to those of the outer C_2 carbons. The same was done for the hydrogen atom bonded to each of the meso carbons, C_m. The coordinates for the single molecule were taken from the Cambridge Crystallographic Data Centre (CCDC).[14] A bare porphyrin molecule exhibits 4-fold symmetry, but due to both the chlorine ligand and the ethyl groups, this is removed in Fe(OEP)Cl.

Testing the importance of the lower symmetry, we first attempted to fit the experimental data with D_4 symmetry on the molecule's structure and force field. The structure used was an ideal 4-fold symmetric model of the molecule. After limited success at fitting the experimental data, we found better results with the lower symmetry CCDC structure. This is consistent

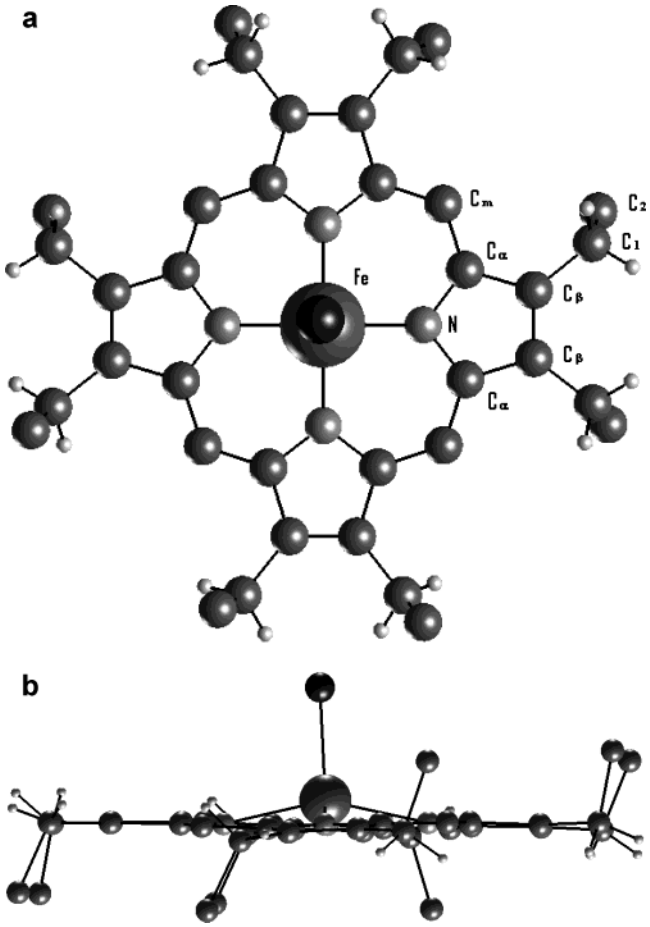

Figure 2. (A) Structure of Fe(OEP)Cl as it was modeled. The small, white atoms are hydrogen. The central atom on top of the iron is the chlorine ligand. The atoms in one quadrant have been labeled. (B) Alternate view of the structure of Fe(OEP)Cl as it was modeled. Notice the irregular orientations of the ethyl groups. From this visual perspective, if they had symmetric orientations, the view of the far ethyl groups would be obstructed by the close ones.

with a previous study on nickel OEP[15] where it is noted that lower frequency RR lines were sensitive to ethyl group orientation.

In the CCDC structure, there is a broken symmetry in both the alignment of the ethyls and the axis of the Fe−Cl bond. The chlorine ligand tilts approximately 3° away from the heme normal. Among the eight ethyls, three point up and five point down in terms of the C_1-C_2 bond, but even within those orientations, there are bond angle variations that further lower the symmetry. The position of the Fe is 0.46 Å above the mean plane of the pyrrole rings, consistent with structure determinations of other 5-coordinated porphyrins.[16] The initial set of Wilson-type force constants was taken from earlier works on porphyrins,[17,18] in particular the stretch and bend constants. Various estimated torsion and out-of-plane constants were added and later refined with the rest of the force field.

We calculated the vibrational modes of our heme molecule using internal coordinates as defined by Wilson et al.[19] The mean square displacements ($\vec{q}_i$) for each atom in the *i*th normal mode were calculated by using[20]

$$\vec{q}_i = \sqrt{\frac{h}{8\pi^2 c\omega_i}\coth\frac{hc\omega_i}{2KT}}\vec{Q}_i \tag{1}$$

Here c is the speed of light, K is Boltzmann's constant, h is Planck's constant, T is the temperature in kelvin, and $\vec{Q}_i$ is one of the $3n$ eigenvectors of the molecular system, where n is the number of atoms. To calculate the probability density of nuclear absorption, only those components of the eigenvectors pertaining to the iron motion are extracted from $\vec{q}_i$, and we call this vector $\vec{u}_i$. Using results from previous discussions of nuclear resonant scattering,[21] the absorption probability density can be written as

$$S_1(E,\hat{k}) = e^{-\langle(k\cdot u)^2\rangle}\sum_{i=1}^{L} e^{\beta E_i/2}\cdot\frac{\Gamma/2\pi}{(E-E_i)^2+\Gamma^2/4}\prod_{j=1}^{L} I_{|n_j|}(C_j(\hat{k})) \tag{2}$$

The first factor depends on the total mean square displacement of the iron atom, summed over all modes. This term and the product including the Bessel function together form the molecular Lamb−Mössbauer factor. The order n_j is equal to the total number of nuclear excitations (+) or deexcitations (−) considered. L is the total number of modes, T is the temperature in kelvin, and I is the Bessel function of the first kind. Assuming only possible contributions from resonant absorption and single phonon excitations, $n_j = 0$ or 1, respectively. $\Gamma = 8$ cm^{-1}, which was the experimental energy resolution. The argument $C_j(\hat{k})$ in the Bessel function is defined as

$$C_j(\hat{k}) = \frac{\langle(\hat{k}\cdot\vec{u}_j)^2\rangle}{\cosh(\beta E_j/2)} \tag{3}$$

Finally, the Fe vibrational density of states (VDOS) is calculated directly as

$$D(E) = 3\frac{E}{E_R}\frac{S_1(E)}{f}[1-e^{-\beta E}] \tag{4}$$

where $E_R = 1.96$ meV is the recoil energy of the nucleus[22] and f is the recoilless fraction.

V. Computational Results and Discussion

A normal-mode calculation of a three-dimensional molecule of n atoms will result in $3n$ eigenvalues and eigenvectors. Of these, six will be of zero frequency to account for linear and angular momentum conservation. For our 58-atom calculation, we had 168 nonzero modes.

The calculation initially used a combination of force constants developed for NiOEP[23] and NiTPP.[18] Results using this preliminary force field showed a need for improved refinement of the force field. This is not too surprising considering the differences in structure of these molecules. NiOEP is a more symmetric structure than Fe(OEP)Cl. There are three common variants depending on the ethyl group arrangement: triclinic A and triclinic B, which have C_{2h} symmetry, and tetragonal C with D_{2d} symmetry.[24] The ethyl groups in those crystalline symmetries are still more symmetric than in Fe(OEP)Cl. Also, without a ligand at the fifth position (bonded to the iron in addition to the four nitrogen atoms) the molecular cores in both NiOEP and NiTPP are planar. With respect to the force field, previous studies did not have metal-specific data to refine to since RR and IR give no metal-specific data at low frequency.

Refinement of the preliminary force field was necessary both to match the known Raman high frequency "marker bands" and to match the new NRVS data. The marker bands are a few non-iron modes at high frequency which are well-known and relatively stable despite slight structural variations. These frequencies were satisfied to within 14 cm^{-1} of their experi-

TABLE 2: Calculated and Previously Observed Raman Marker Band Frequencies

mode label	calcd freq (cm^{-1})	measd freq[a] (cm^{-1})
ν_{10}	1649	1637−1655
ν_2	1616	1592−1602
ν_{11}	1569	1568−1577
ν_3	1495	1503−1520
ν_4	1395	1378−1383
$\nu(C_1–C_2)$	1009	1023−1024

[a] Lower values from CuOEP[37] and higher values from NiOEP[22] studies.

mental values in similar molecules[23] (Table 2). The refinement procedure was based on the Jacobian determinant method.[25] The problem of refining several hundred force constants while using the marker bands and the NRVS spectrum's frequencies and amplitudes is mathematically underconstrained. Note that 36% of all calculated modes are found in the energy range of the NRVS data (Figure 3). For that reason it was necessary to place limits on force constants to avoid unphysical values. A comparison of the final result of the calculation with the experimental NRVS data is given in Figure 1.

The largest discrepancies between the calculated and the experimental results are in the amplitudes of a series of features below 100 cm^{-1}, one at 143 cm^{-1}, and one at 357 cm^{-1}. There is a trend among the modes giving rise to these features. The one at 143 cm^{-1} is a mode due to ethyl vibrations, and all of the others are out-of-plane vibrational modes. We believe that the amplitudes of these modes involving the ethyl substituents, the chlorine ligand, and low frequency out-of-plane motions (which tend to be global vibrations) in the crystalline sample are reduced by intermolecular effects. It can be seen from the crystal structure[14] that there are 60 instances where interatomic distances are below 5 Å. The chlorine ligand is roughly 4 Å from the nearest neighboring molecule, and several outer carbon atoms are within 3.5 Å of neighboring molecules. In our single-molecule model, this coupling, and resulting dispersion, was not considered.

The calculated modes can be compared to the normal modes of the 37-atom porphyrin core ($FeC_{32}N_4$) D_{4h} macrocycle as developed by Li et al. for Ni(OEP).[17,24] In this classification scheme, there are 53 possible in-plane modes denoted by ν_i, and 26 out-of-plane modes denoted by γ_j. These are a subset of the 105 nonzero modes corresponding to $3n - 6$ vibrational degrees of freedom. Assuming a D_{4h} symmetric metalloporphyrin skeleton, we can separate these into in-plane and out-of-plane displacements. There are $2n - 3 = 71$ in-plane and $n - 3 = 34$ out-of-plane modes. Classified according to the irreducible representation of the D_{4h} point group, these are

$$\gamma_{op} = 3A_{1u} + 6A_{2u} + 5B_{1u} + 4B_{2u} + 8E_g \quad (5)$$

$$\nu_{ip} = 9A_{1g} + 8A_{2g} + 9B_{1g} + 9B_{2g} + 18E_u \quad (6)$$

where E modes are doubly degenerate modes. Iron displacement only occurs in E_u and A_{2u} modes, and neither of these are Raman active. All other modes have no contribution to the iron displacement. In practice, however, we find that the broken D_{4h} symmetry in the 5-coordinated octaethylporphyrin allows mode mixing to take place. With this symmetry lifted, modes measured by NRVS include modes that may be Raman active. Another consequence of the lower symmetry is that several of the degenerate modes such as ν_{50} and ν_{53} from the D_{4h} symmetric system become doublets in the real system (Table 3).

Using the same initial set of force constants as for Fe(OEP)-Cl, the normal modes of a 33-atom core were calculated. This is the same as the Li et al. 37-atom core, but with the hydrogen atoms at the C_m sites not explicitly included; instead their masses were added to that of the C_m atom. (Recall that this was done in the Fe(OEP)Cl calculation as well.) Attached to the C_β sites were carbon atoms, since that is what Fe(OEP)Cl has. The 33-atom porphyrin core vibrations are each defined by a core eigenvector, which describes the motion of all core atoms in each normal mode. It should be noted here that the labels we give these $3n - 6 = 93$ modes correspond to the labels that Li et al. used for equivalent modes of the 37-atom core porphyrin. To quantifiably compare the mode characters of Fe(OEP)Cl with the modes of the 33-atom core, we take the inner product of the core eigenvectors with our calculated modes. The more a calculated mode resembles a particular core mode, the higher the inner product. It was found that as the porphyrin becomes more complex with the addition of the iron ligand and ethyl groups, mixing of the core modes takes place. In Fe(OEP)Cl there is such strong mixing that it is of limited utility to describe the actual modes in terms of the porphyrin core modes. When we describe a mode as primarily being a ν_{53} mode, for example, the largest inner product between the true mode and a porphyrin core mode was the ν_{53} mode, even though the percentage overlap might be well under 50%.

Table 3 shows the character and breakdown of the NRVS frequencies according to the aforementioned scheme. Fe−Cl stretch and N−Fe−Cl bend are two non-core modes of interest which are also included in the table. It should be noted that the NRVS peaks are each made up of several vibrational modes, so there is not a one-to-one mapping of an NRVS peak to a mode with a specific character. The frequencies and amplitudes of each calculated mode are plotted in Figure 3, along with the final spectrum obtained by convolution with the instrumental resolution function. Of these individual modes, the ones with the largest amplitudes are listed in Table 3.

Besides comparing to core porphyrin vibrational modes, normal-mode vibrations may alternatively be classified by a potential energy distribution (PED) among internal coordinates (bond stretches, angle bends, torsional or dihedral stresses) during a particular normal-mode vibration. This is done by transforming our calculated atomic displacements from mass-weighted Cartesian coordinates to internal coordinates. From Hooke's law each internal coordinate has a potential energy contribution of the form

$$PE = (1/2)F_{ij}s_is_j \quad (7)$$

where F_{ij} is an element of the force matrix and s_i is a displacement of one of the internal coordinates defined as

$$\vec{s} = B\vec{q} \quad (8)$$

Here B is the transformation matrix from mass-weighted Cartesian to internal coordinates. The PED results are tabulated in Table 3. The PED identifies which chemical bonds are sustaining the most stress or storing the most energy for a particular normal mode.

The kinetic energy distribution (KED) was also calculated to aid in the understanding of the individual normal modes (Table 4). Analogous to the PED, the KED indicates which particular atoms contain the most kinetic energy in a given vibrational mode. The KED for atom i is given by

$$KED_i = (1/2)m_iv_i^2 \quad (9)$$

The values in the table are listed according to percentage

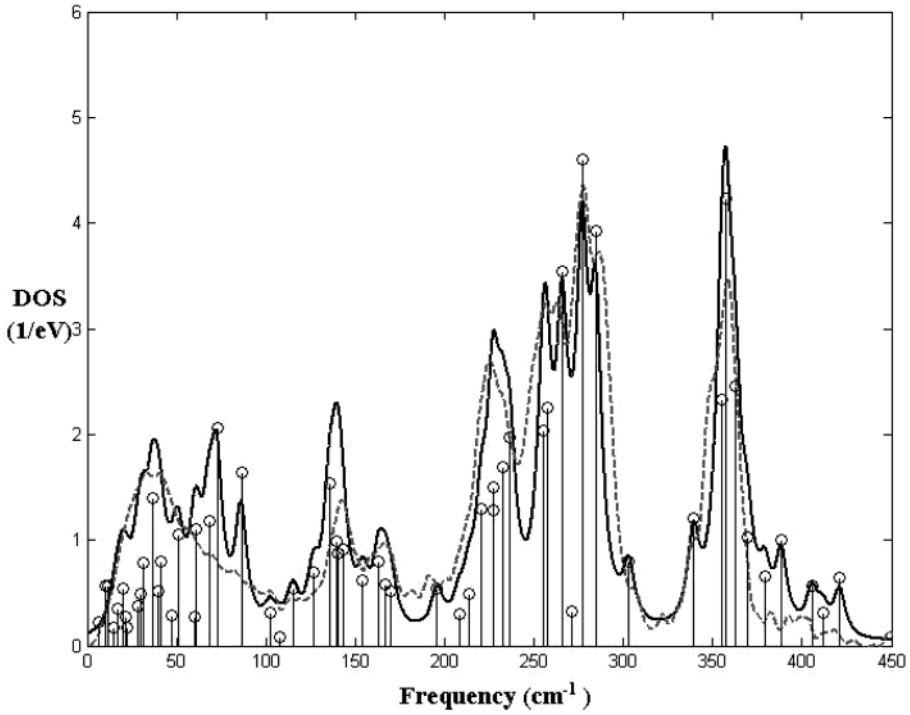

Figure 3. Contributions from individual modes to calculated density of states. In the density of states, each of the modes is given an 8 cm^{-1} Lorentzian line width. Dashed line is experiment; solid line is calculation.

TABLE 3: Percentage Overlap of Calculated Modes at $T = 87$ K with Porphyrin Core Normal Modes and Ligand Vibrations[a]

freq (cm^{-1})	assgnt	Fe−Cl str	Cl−Fe−N bend[b]	37-atom core modes[c]											
				ν_{50a}	ν_{50b}	ν_{51a}	ν_{51b}	ν_{52a}	ν_{52b}	ν_{53a}	ν_{53b}	γ_6	γ_7	γ_8	γ_9
36	γ_7/γ_9	–	–	–	–	–	–	–	–	–	–	10.3	22.2	–	27.7
51		–	–	–	–	–	–	–	–	–	–	–	4.9	3.7	5.2
61		–	2.1	–	–	–	–	–	–	–	–	–	–	4.2	–
68		–	2.6	–	–	–	–	–	–	–	–	–	–	10.3	–
72		–	–	–	–	–	–	–	–	–	–	–	–	34.1	–
86	γ_8	–	–	–	–	–	–	–	–	–	–	–	11.5	37.7	–
135	ν_{51a}	–	–	–	–	42.9	5.1	–	–	4.3	–	–	–	–	–
143	ν_{51b}	–	–	–	–	16.3	11.3	–	–	–	–	–	–	–	–
220	γ_6	7.1	10.2	–	–	–	–	–	–	–	–	32.6	7.9	–	–
227	ν_{52a}/ν_{52b}	–	4.9	8.6	4.6	–	–	44.2	27.7	–	3.4	–	–	–	–
232	Cl−Fe−N	–	11.6	–	3.5	–	–	–	–	2.9	–	–	–	–	–
236		–	6.1	5.4	–	–	–	6.2	10.1	–	7.8	6.6	–	–	–
255		–	–	–	4.1	–	–	–	13.5	16.8	–	–	–	–	–
257		–	–	–	4.1	–	–	–	27.5	23.0	–	–	–	–	–
265	ν_{53b}	–	–	9.8	–	–	–	21.8	–	–	37.8	–	–	–	–
277	ν_{50b}/ν_{53a}	–	2.3	–	50.2	4.1	–	–	–	34.6	3.4	2.8	3.8	–	–
284	ν_{50a}	–	–	52.4	–	–	3.4	–	–	–	24.1	–	–	–	–
354		10.8	–	5.3	–	–	–	–	–	3.7	10.5	3.9	–	3.0	–
357	Fe−Cl/γ_6	60.2	7.3	–	–	–	–	–	–	–	2.9	15.5	9.4	13.1	4.3
362		13.5	–	–	6.5	–	–	–	–	10.6	–	18.4	4.5	–	–

[a] A dash indicates either less than 2% overlap with core modes, very little iron displacement (2% of largest mode), or both. [b] There are four independent Cl−Fe−N bend coordinates. Listed at each frequency is the average of the four coordinates. [c] Modes are calculated using a 33-atom core which does not explicitly include the hydrogen atoms at the C_m sites, but are labeled according to the 37-atom core (see text).

contribution by each atom for a given normal mode. Thus, summing all an atom's contributions for a given mode gives 100%.

VI. Mode Assignments

A. In-Plane Modes. D_4 symmetric porphyrins only have in-plane iron displacement in modes of symmetry type E_u. With the breaking of that symmetry, the usual double degeneracy of these modes splits. Of all E_u modes, few of them fall in the frequency range of our NRVS data. This subset includes modes corresponding to ν_{50} to ν_{53} of the 37-atom porphyrin core.

In the core mode ν_{50} the iron moves toward one pyrrole ring, and away from the opposite pyrrole. In effect, this stretches one Fe−N bond, compresses another, and leaves the other two relatively unaffected. Our largest overlap with core mode ν_{50} is split between modes at 277 and 284 cm^{-1}. It is evident from the PED (Table 4) that these modes store the most energy in the Fe−N stretch coordinate. This mode was observed by Li et al. to be split between 341 and 355 cm^{-1} while using RR on tetragonal crystals of NiOEP.[17] The same mode was measured at 420 cm^{-1} in NiP.[17] This indicates that it is a mode that is sensitive to substituents. To explain the lower frequency, it should be noted that our molecule is an Fe(III) porphyrin and not a Ni(II) porphyrin, and that the iron is situated out of the plane of the molecule. The nonplanar orientation of the Fe−N bond reduces the effective force for in-plane motions from what

TABLE 4: Potential Energy Distribution, Kinetic Energy Distribution, and Iron Amplitude (in pm) for the Calculated Modes[a]

freq (cm^{-1})	assignment	Fe disp (pm)	PED (%)	KED (%)
36	γ_7/γ_9	1.92	global	C_β (31.8) + C_2 (47.5)
51		1.18	δ(ClFeN) (13.1) + $\tau(C_\beta C_\beta C_1 C_2)$ (25.7)	Cl (23.6) + C_β (22.7) + C_2 (32.0)
61		1.10	$\delta(FeNC_\alpha)$ (12.6) + δ(ClFeN) (27.0)	Cl (33.5) + C_α (16.6) + C_m (21.1) + C_2 (14.3)
68		1.12	δ(ClFeN) (34.4) + $\delta(FeNC_\alpha)$ (14.6)	Cl (45.7) + C_α (17.9) + C_m (24.5)
72		1.88	δ(ClFeN) (10.3)	Cl (12.6) + C_α (17.0) + C_m (21.3) + C_2 (25.9)
86	γ_8	1.37	$\tau(C_\alpha C_\beta C_1 H_E)$ (10.3)	C_α (21.6) + C_m (26.9) + C_2 (23.4)
135	ν_{51a}	1.02	$\nu(C_\alpha C_\beta)$ (11.7) + $\delta(C_\beta C_\beta C_1)$ (11.7)	C_β (16.8) + C_1 (37.0) + C_2 (15.1) + H_E (17.0)
163	ν_{51b}	0.49	ν(FeN) (12.7) + $\tau(C_\beta C_\beta C_1 C_2)$ (12.8)	N (10.9) + C_α (15.8) + C_β (28.3) + C_1 (15.6) + C_2 (19.3)
220	γ_6	0.67	ν(FeCl) (15.8) + δ(NFeN) (21.5)	Cl (22.1) + N (43.2) + C_α (10.8)
227	ν_{52a}/ν_{52b}	0.77	$\delta(C_\beta C_\beta C_1)$ (27.6) + $\delta(C_\alpha C_\beta C_1)$ (10.6)	C_β (13.1) + C_1 (37.5) + H_E (23.0)
232	Cl−Fe−N bend	0.86	$\delta(FeNC_\alpha)$ (12.7) + δ(ClFeN) (12.3) + $\tau(NC_\alpha C_m C_\alpha)$ (33.6)	N (49.9) + C_α (32.1)
236		0.99	$\delta(C_\beta C_\beta C_1)$ (12.5) + $\tau(NC_\alpha C_m C_\alpha)$ (14.0)	N (22.5) + C_α (21.4) + C_1 (18.9) + H_E (11.4)
255		0.99	$\delta(C_\alpha C_\beta C_1)$ (14.1) + $\delta(C_\beta C_\beta C_1)$ (42.9)	C_β (10.2) + C_1 (39.0) + H_E (27.6)
257		1.08	$\delta(C_\alpha C_\beta C_1)$ (12.2) + $\delta(C_\beta C_\beta C_1)$ (31.9)	Fe (10.3) + C_β (13.3) + C_1 (34.3) + C_2 (11.0) + H_E (24.0)
265	ν_{53b}	1.67	$\delta(FeNC_\alpha)$ (12.9) + $\delta(C_\beta C_\beta C_1)$ (10.1)	Fe (25.4) + C_α (11.6) + C_β (16.4) + C_1 (18.9) + H_E (11.8)
277	ν_{50b}/ν_{53a}	2.13	ν(FeN) (33.3)	Fe (42.7) + C_β (12.7) + C_1 (13.6) + C_2 (11.8)
284	ν_{50a}	1.80	ν(FeN) (30.1) + $\delta(C_\beta C_\beta C_1)$ (16.6)	Fe (31.1) + C_β (15.3) + C_1 (21.9) + C_2 (10.3) + H_E (13.3)
354		0.96	$\delta(C_\beta C_1 C_2)$ (37.3)	Fe (11.0) + C_β (25.2) + C_2 (28.2)
357	Fe−Cl stretch/γ_6	1.72	ν(FeCl) (51.6) + $\delta(C_\beta C_1 C_2)$ (13.2)	Fe (36.1) + Cl (27.4) + C_β (10.5) + C_2 (10.1)
362		0.99	ν(FeCl) (11.2) + $\delta(C_\beta C_1 C_2)$ (34.4)	Fe (12.2) + C_β (27.2) + C_2 (25.5)

[a] Listed as percentages of the total energy of a particular mode. Modes with 10% or greater contribution are listed. The term "global" means no individual contribution as large as 10%. Values listed are the sum of the contributions from all four quadrants.

it would have been if this displacement were along the bond, leading to a reduction in frequency. We confirmed this by recalculating the modes with the iron in the plane of the molecule, and found that the ν_{50} and ν_{53} modes were upshifted by 15−30 cm^{-1}.

The core mode ν_{51} is an in-plane mode in which the C_β−C_1 bonds in the ethyl groups bend asymmetrically. (Recall that our core molecule incorporated carbons at the β site.) The equivalent core mode with a symmetric bend of the same bond is the ν_{52} mode. The ν_{51} mode was calculated to be at 299 cm^{-1} by Piffat et al.[23] in NiOETPP, and at 317 cm^{-1} in NiOEP. Although our calculation shows overlap with modes at 277 and 284 cm^{-1}, there is a much larger contribution at a pair of modes at 135 and 143 cm^{-1}. The ν_{52} mode was calculated by the same group to fall at 293 cm^{-1}, but it was observed at 263 cm^{-1} in NiOEP. Our calculation shows the largest ν_{52} contributions at 227, 257, and 265 cm^{-1}.

Despite having a reasonable match to experimental frequencies for the ν_{51} and ν_{52} modes, we question the utility of describing these ethyl-related modes in terms of the 37-atom, symmetric core molecule's modes. The largest break in D_4 symmetry in our molecule involves the ethyl groups. If one considers a particular ethyl mode and then rotates that ethyl group with respect to the rest of the molecule, it is easy to see that the symmetry type of the mode within the molecule will change. It is therefore more informative to look at the PED (Table 4). The predominant energy in both ν_{51} and ν_{52} modes should be contained in bending modes which include the C_1 ethyl carbon atom and the C_β outer pyrrole atom, the third atom being either C_α or C_β. There are several modes in a range from 135 to 284 cm^{-1} which satisfy this.

The ν_{53} mode in the core porphyrin has the largest overlap with our modes at 265 and 277 cm^{-1}. For comparison, this mode was calculated at 167 cm^{-1}, yet measured at 212 cm^{-1} in NiOEP,[24] observed at 282 cm^{-1} in NiP,[17] and calculated using both empirical force field and SQM force field methods at 307 and 325 cm^{-1}, respectively, in NiTPP.[18] As with the ν_{50} mode, the variation in iron charge state and the nonplanarity of the molecule probably account for the differences.

B. Out-of-Plane Modes. D_4 symmetric porphyrins only have out-of-plane iron displacement in modes of symmetry type A_{2u}. Unlike E_u modes, these modes are not degenerate. Out-of-plane modes which fall in the frequency range of our NRVS data include modes γ_6−γ_9.

Normal modes are the pathways to binding, dissociation, and conformational change in molecules.[26,27] Biologically significant modes in hemes are ones which contain out-of-plane motion of the iron atom. They are significant because it is believed that the Fe atom binds and dissociates O_2, CO, and other such molecules along this pathway. The purest core mode with this type of motion is referred to as γ_9, and is usually termed the "doming" mode. It is the lowest frequency, out-of-plane motion of the molecule that has iron displacement,[28,29] and visually makes the entire molecule dome up and down like a circular membrane at its fundamental frequency. One way the iron atom extends out to its biological environment is via this doming mode.[30] The doming mode has been experimentally elusive since very low frequency modes are difficult to detect in RR experiments. In contrast, NRVS is most sensitive to low frequency modes because of the enhanced Fe amplitude. The mode is IR active, but since it is a highly delocalized mode involving the motion of a large number of atoms, isotopic substitution still leaves the assignment ambiguous. A normal-mode study on a 4-coordinated heme by Li et al.[31] predicted the doming mode to be at 32 cm^{-1} in NiOEP. More recent studies by Kozlowski et al.[32] found that it is strongly dependent on the spin state of the iron. They calculated it to be between 63 and 98 cm^{-1} on various 4- and 5-coordinated iron(II) porphines.

These variations are in part due to lack of experimental evidence which would allow for a confident assignment. NRVS provides more compelling evidence to make a confident assignment of this mode since it involves significant iron displacement. Our calculations find the mode with the most γ_9

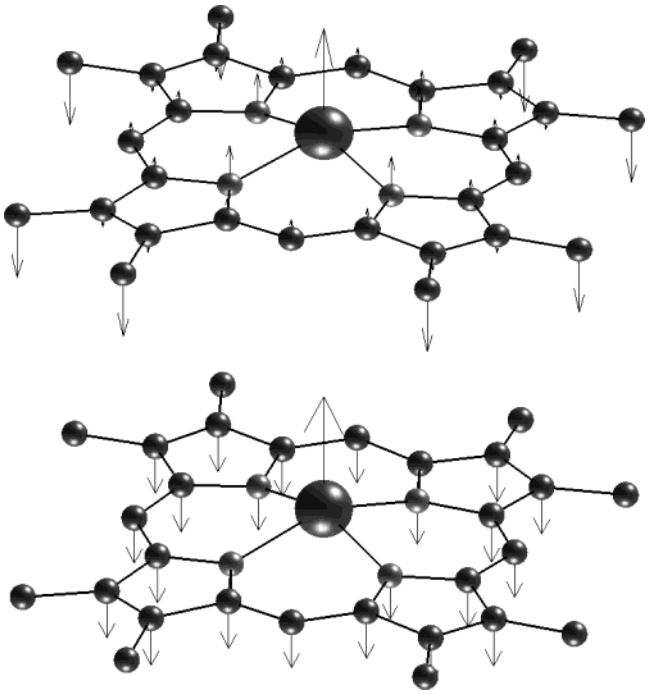

Figure 4. Comparison of calculated γ_9 mode used in this study (top) to γ_9 mode used in previous studies referred to in section VIB (bottom). That mode did not include motion of the C_β substituents.

character at 36 cm^{-1}. A previous NRVS study calculated the γ_9 mode at 75 cm^{-1} in Fe(TPP)NO.[5] However, that study defined the γ_9 mode in a different manner as compared to the present work. The study of Fe(TPP)NO described the γ_9 mode as the motion of iron in one out-of-plane direction with the rest of the core atoms moving in the other, following a description of the mode in a study by Kozlowski et al.[33] The present study has used the actual, calculated eigenmode of a 33-atom core. For a comparison of the two modes, see Figure 4. With this in mind, we recalculated the overlap using the other γ_9 definition, and found that we have the greatest overlap with that mode at 86 cm^{-1}—not so different from their result in Fe(TPP)NO. A study on Fe(TPP)(2-MeHIm)[6] was done using that same description of the γ_9 mode and also found the γ_9 mode at higher frequency (67 and 79 cm^{-1}), but it should be noted that the modes at 25, 32, and 33 cm^{-1} in that same study (which were classified as phenyl modes) contained much doming γ_9 character. In fact, those modes in the absence of phenyl substituents match the character of our calculated γ_9 mode very well. In the present study, the low frequency modes similarly contained motion of the C_β substituents, which in this case are ethyl groups. This is evident from the KED (Table 4).

It is significant that the doming mode is found at low frequency, because in large proteins such as myoglobin, major vibrational modes occur at low frequencies which can overlap with the iron modes. These modes tend to be around 30 cm^{-1}.[34]

Other out-of-plane modes of interest are the γ_6, γ_7, and γ_8. The γ_6 mode is a symmetric pyrrole folding. The iron, nitrogen, and C_β atoms move upward out of the plane while the C_α atoms move downward, thus creating a fold about a line through the C_α atoms. Three different modes have γ_6 character (Table 3). The γ_7 mode is a mode characterized primarily by an out-of-plane motion of the C_m atoms contrary to the C_α atoms. The γ_8 mode is characterized by motion of the iron atom and the C_1 atoms moving upward while the rest of the core atoms move downward. Both γ_7 and γ_8 contribute significantly to a mode at 86 cm^{-1}, but γ_7's largest contribution corresponds to the same 36 cm^{-1} that is primarily γ_9 in character. It is interesting to note that this mode at 36 cm^{-1}, if viewed in terms of the PED, has a global distribution of energy, so even though the iron is undergoing large displacement out of the plane of the molecule, no single bond in particular is being stressed to accomplish this. This relative stability, and broad distribution of KED as well, makes it a choice candidate for coupling to a protein mode.

In the region below 100 cm^{-1} where most of the out-of-plane modes exist, most of the calculated modes cannot be seen in the experimental data. This is presumably due to intermolecular coupling, which creates dispersion in the data in this frequency range. Since our calculation is based on a single molecule, it cannot account for these effects or for contributions from acoustic modes. The effect in the data is that we calculate larger amplitude, discrete lines which get washed out in the crystalline sample data.

C. Chlorine Modes. Chlorine ligand modes include both the stretching and the bending of the Fe−Cl bond. The mode at 357 cm^{-1} is predominantly a stretch between Fe and the ligand Cl. It is 60.2% pure Fe−Cl stretch. The ones at 354 and 362 cm^{-1} also contain much of the same character. The stretching mode between Fe and Cl was observed at 364 cm^{-1} in RR experiments by Kitagawa et al.[35] This mode was also measured via IR in Fe(OEP)Cl at 357 cm^{-1} by Ogoshi et al.[36] It is interesting to note that the relatively high frequency Fe−Cl stretch mode also has contributions from all of the out-of-plane modes γ_6−γ_9. This suggests that although γ_9, the doming mode, is generally assumed to be the most biologically significant mode in terms of ligand binding, there may be other pathways to binding by having modes at very different frequencies being coupled to γ_9 motion.

The chlorine bending mode has its largest contribution at 232 cm^{-1} with another relatively large contribution at 220 cm^{-1}. These modes coincide with the chlorine bending in one direction in the mode at 220 cm^{-1}, and in an orthogonal direction at 232 cm^{-1}. This is due to the nonsymmetric location of the chlorine atom and the breaking of D_4 symmetry in the force field.

VII. Conclusion

The new NRVS data have afforded us the possibility of characterizing many low frequency vibrational modes with iron participation. The experimental NRVS data and the calculated results match very well. These data provide more constraints than other forms of spectroscopy, since they contain iron-specific amplitude information in addition to frequency information. The high frequency Raman marker bands are also satisfied. We confidently assign many previously unassigned low frequency modes such as the γ_9 doming mode. It was learned from this study that the language of describing normal modes of all porphyrins in terms of porphyrin core modes—as has been the convention—loses its utility as the model compounds become more complex and less symmetric. It is seen that all of the modes in Fe(OEP)Cl are hybridized modes of the core. In only two of the modes of Fe(OEP)Cl was there greater than 50% overlap with a core mode.

There is potential biological significance in ligand modes at hundreds of wavenumbers being hybridized with low frequency out-of-plane modes such as the conventional doming mode. This coupling seems to imply the ability of heme ligands to bind to the iron site via pathways other than these low frequency modes. This model compound study leads us to potentially greater understanding of the role of heme molecules in proteins.

TABLE 5: List of Acronyms Used

acronym	definition
DOS	density of states
KED	kinetic energy distribution
NRVS	nuclear resonance vibrational spectroscopy
OEP	octaethylporphyrin
OETPP	octaethyltetraphenylporphyrin
PED	potential energy distribution
TPP	tetraphenylporphyrin
2-MeHIm	2-methylimidazole

Acknowledgment. This work is supported in part by the Mobile Manufacturer's Forum, in part by the NSF through Award No. PHY-9988763 (for T.E.B., E.W.P., and S.M.D.) and Award No. PHY-99-83100 (J.T.S.), and by the NIH through Grant GM-52002 (J.T.S.). Use of the Advanced Photon Source was supported by the U. S. Department of Energy, Basics Energy Sciences, Office of Science, under Contract No. W-31-109-Eng-38.

References and Notes

(1) Banaszak, L. J. *Foundations of Structural Biology*; Academic: San Diego, 2000; p 137.

(2) Dolphin, D. *The Porphyrins*; Academic: New York, 1978; Vol. 7.

(3) Feher, G.; Okamura, M. Y. *The Photosynthetic Bacteria*; Clayton, R. K., Ed.; Plenum: New York, 1978; pp 349−386.

(4) Moens, L.; Dewilde, S. *Nature* **2000**, *407*, 461−462.

(5) Rai, B. K.; Durbin, S. M.; Prohofsky, E. W.; Sage, J. T.; Wyllie, G. R. A.; Scheidt, W. R.; Sturhahn, W.; Alp, E. E. *Biophys. J.* **2002**, *82*, 2951−2963.

(6) Rai, B. K.; Durbin, S. M.; Prohofsky, E. W.; Sage, J. T.; Wyllie, G. R. A.; Scheidt, W. R.; Sturhahn, W.; Alp, E. E. *Phys. Rev. E* **2002**, *66*, 051904.

(7) Seto, M.; Yoda, Y.; Kikuta, S.; Zhang, X. W.; Ando, M. *Phys. Rev. Lett.* **1995**, *74*, 3828.

(8) Keppler, C. *Eur. Biophys. J. Biophys.* **1997**, *25*, 221.

(9) Chumakov, A. I.; Sturhahn, W. *Hyperfine Interact.* **1999**, *123*, 781.

(10) Sturhahn, W.; Toellner, T. S.; Alp, E. E.; Zhang, X.; Ando, M.; Yoda, Y.; Kikuta, S.; Seto, M.; Kimball, C. W.; Dabrowski, B. *Phys. Rev. Lett.* **1995**, *74*, 3832.

(11) Sage, J. T.; Paxson, C.; Wyllie, G. R. A.; Sturhahn, W.; Durbin, S. M.; Champion, P. M.; Alp, E. E.; Scheidt, W. R. *J. Phys.: Condens. Matter* **2001**, *13*, 7707−7722.

(12) Toellner, T. S.; Hu, M. Y.; Sturhahn, W.; Quast, K.; Alp, E. E. *Appl. Phys. Lett.* **1997**, *71*, 2112−2114.

(13) Sturhahn, W.; Kohn, V. G.; Alp, E. E. *Hyperfine Interact.* **1999**, *123*, 367.

(14) Senge, M. O. Private communication to the CCDC, 1997.

(15) Li, X. Y.; Czernuszewicz, R. S.; Kincaid, J. R.; Spiro, T. G. *J. Am. Chem. Soc.* **1989**, *111*, 7012−7023.

(16) Ellison, M. K.; Scheidt, W. R. *J. Am. Chem. Soc.* **1997**, *119*, 7404−7405.

(17) Li, X. Y.; Czernuszewicz, R. S.; Kincaid, J. R.; Su, Y. O.; Spiro, T. G. *J. Phys. Chem.* **1990**, *94*, 31−47.

(18) Rush, T. S.; Kozlowski, P. M.; Piffat, C. A.; Kumble, R.; Zgierski, M. Z.; Spiro, T. G. *J. Phys. Chem. B* **2000**, *104*, 5020−5034.

(19) Wilson, E. B.; Decius, J. C., Jr.; Cross, P. C. *Molecular Vibrations*; Dover: New York, 1980; pp 54−63.

(20) Cyvin, S. J. *Molecular Vibrations and Mean Square Amplitudes*; Elsevier Publishing: Amsterdam, 1968.

(21) Paulsen, H.; Winkler, H.; Trautwein, X.; Gruensteudel, H.; Rusanov, V.; Toftlund, H. *Phys. Rev. B* **1999**, *59*, 975−984.

(22) *Moessbauer Effect Data Index*; Stevens, J. G., Stevens, V. E., Eds.; IFI/Plenum: NewYork, 1975.

(23) Piffat, C.; Melamed, D.; Spiro, T. G. *J. Phys. Chem.* **1993**, *97*, 7441−7450.

(24) Li, X. Y.; Czernuszewicz, R. S.; Kincaid, J. R.; Stein, P.; Spiro, T. G. *J. Phys. Chem.* **1990**, *94*, 47−61.

(25) *Vibrational Spectra and Structure*; Levin, I. W., Pearce, R. A. R., Durig, J. R., Eds.; Elsevier Scientific: New York, 1975; Vol. 4, p 102.

(26) Xie, A.; van der Meer, A. F. G.; Austin, R. H. *Phys. Rev. Lett.* **2002**, *88*, 018102-(1-4).

(27) Leach, A. R. *Molecular Modelling Principles and Applications*, 2nd ed.; Pearson Education Limited: Essex, England, 2001; pp 273−278.

(28) Hoard, J. L.; Scheidt, W. R. *Proc. Natl. Acad. Sci. U.S.A.* **1973**, *70*, 3919−3922.

(29) Perutz, M. *Nature* **1970**, *228*, 726−739.

(30) Sage, J. T.; Durbin, S. M.; Sturhahn, W.; Wharton, D. C.; Champion, P. M.; Hession, P.; Sutter, J.; Alp, E. E. *Phys. Rev. Lett.* **2001**, *113*, 4966−4969.

(31) Li, X. Y.; Zgierski, M. Z. *Chem. Phys. Lett.* **1992**, *188*, 16−20.

(32) Kozlowski, P. M.; Spiro, T. G.; Zgierski, M. Z. *J. Phys. Chem. B* **2000**, *104*, 10659−10666.

(33) Kozlowski, P. M.; Spiro, T. G.; Berces, A.; Zgierski, M. Z. *J. Phys. Chem. B* **1998**, *102*, 2603−2608.

(34) Achterhold, K.; Keppler, C.; Osterman, A.; van Buerck, U.; Sturhahn, W.; Alp, E. E.; Parak, F. G. *Phys. Rev. E* **2002**, *65*, 051916.

(35) Kitagawa, T.; Abe, M.; Kyogoku, Y.; Ogoshi, H.; Watanabe, E.; Yoshida, Z. *J. Phys. Chem* **1976**, *80*, 1181−1186.

(36) Ogoshi, H.; Watanabe, E.; Yoshida, Z.; Kincaid, J.; Nakamoto, K. *J. Am. Chem. Soc.* **1973**, *95*, 2845.

(37) *Porphyrin Handbook*; Kincaid, J. R., Kadish, K. M., Smith, K. M., Guilard, R., Eds.; Academic Press: 1999; Vol. 7, Chapter 51, p 266.